Asia Pacific Academy of Science Pte. Ltd.

Computer and Telecommunication Engineering 2024, 2(1), 2368.
https://doi.org/10.54517/cte.v2i1.2368

Article

Slot fed circularly polarized magneto-electric dipole antenna array fed by optimized printed microstrip gap waveguide network

Abdelmoniem T. Hassan, Ahmed A. Kishk*

Department of Electrical and Computer Engineering, Concordia University, Montreal, QC H3G 1M8, Canada
*** Corresponding author:** Ahmed A. Kishk, ahmed.kishk@concordia.ca

CITATION

Hassan AT, Kishk AA. Slot fed circularly polarized magneto-electric dipole antenna array fed by optimized printed microstrip gap waveguide network. Computer and Telecommunication Engineering. 2024; 2(1): 2368. https://doi.org/10.54517/cte.v2i1.2368

ARTICLE INFO

Received: 6 November 2023
Accepted: 1 March 2024
Available online: 25 March 2024

Abstract: A compact, circularly polarized 8 × 8 antenna array is designed for the 60 GHz band. The array comprises circularly polarized magneto-electric dipoles (CP-ME-Dipole) excited by narrow slots. The slots are fed by a printed gap waveguide (PGWG) cooperative network optimized based on the termination of the effective impedance of the array elements. Thus, it accounts for the space mutual coupling of the antenna elements. A procedure based on the full-wave analysis of a 4 × 4 array is used to estimate each element's 8 × 8 array effective port impedance. The cooperative feeding network is designed based on the known effective impedances. The array is divided into two half subarrays out of phase from each other, and a rectangular waveguide feeds both sides. The commonly measured bandwidth of 18.3% achieves return loss better than 10 dB and an axial ratio below 3 dB (AR) of less than 3 dB. A maximum gain of 26.2 dBic with a high radiation efficiency of 82% radiation efficiency.

Keywords: 5G; mmWave antenna array; circular polarization; printed gap waveguide; magneto-electric dipole

1. Introduction

The unlicensed frequency band 57–64 GHz has been of interest for radio frequency (RF) and antenna arrays. Many potential applications are possible for such a band (V-band) [1], which requires new technology to provide stable performance and connectivity. To achieve these goals, new components are needed for wireless communications systems. Operating at mm-wave (V-band) provides the broad bandwidth required to meet 5G requirements [2]. However, the 60 GHz band suffers from high atmospheric absorption. Therefore, it requires high-gain antennas at the physical layer of the communication system [3].

Mobile terminals are expected to operate in the mm-wave range for the Internet of Things (IoT) and high-speed communications [2]. Thus, significant research studies have been conducted for communication applications [4,5], such as microbase stations covering only hundreds of meters of cells that are supposed to communicate directly with the users with almost no multipath environments. Therefore, the signals have to be of high gain and narrow beamwidth to overcome the high attenuation of the mm-wave signals.

The multipath propagation effect can be reduced significantly when a circular polarization is used [6]. As a result, a high-gain antenna array at 60 GHz with circular polarization is a proper candidate to enhance channel communication performance. However, at mm-wave frequencies, the required dimensions are relatively small, and consequently, the fabrication complexity increases, affecting its performance. In terms of performance, high efficiency, and low losses, antenna array structures must

compensate for the free space path loss [3], which is not complicated. However, the corporate feeding network is usually a major source of losses at mm-wave frequencies. Therefore, the feeding network must be implemented using the proper electromagnetic guiding technology. For instance, the metal waveguide can provide high gain and efficiency when using slots [7,8]. Still, at mm-wave, the challenges are in fabrication, where electrical contacts between the metal parts of the waveguide structure must be assured. Substrate integrated waveguide (SIW) [9] technology has been successfully used at mm-wave frequencies to design a high-gain antenna array [10–16], but the dielectric losses degrade the efficiency and the radiation performance. In addition, the SIW width makes it difficult to have a feeding network that directly feeds the array elements that are tightly spaced. Alternately, a new gap in waveguide technology is introduced to overcome these limitations [17,18].

The theoretical concept of the gap waveguide is based on two perfect electric conductors (PEC-PEC) parallel plates where the signal can propagate. Suppose the bottom plate is laid on a perfect magnetic conductor (PEC-PMC) layer, and the two plates are separated by a gap smaller than a quarter wavelength. Thus, it suppresses any wave with any polarization from propagating between PEC-PMC plates. Therefore, vertically polarized waves are confined between the PEC-PEC parts of the two parallel plates. A periodic texture with a high surface impedance realizes the bottom PMC layer. These periodic textures provide a stop frequency band where the bottom layer can perform as PMC. Therefore, it is called an artificial magnetic conductor (AMC), which must be designed for a particular frequency band that easily has a 1:2 bandwidth. Different realizations of the AMC layer end up in different gap waveguide structures: ridge, groove, and microstrip ridge gap waveguide (MRGW) [19]. Among these different structures of the gap waveguides, MRGW offers more design flexibility in designing a complicated feeding network by avoiding disturbing the periodic structure of the AMC layer.

At 60 GHz, several circularly polarized (CP) antenna array designs have been reported. A simple planar antenna array was introduced using a patch antenna as a radiating element; besides the low efficiency, the 3-dB axial ratio (AR) is less than 10% [20,21]. A circular-polarized array antenna using hexagonal radiating apertures using a metal waveguide feeding network was proposed [22]. Although high gain and efficiency were achieved, a narrow 3-dB AR was obtained, aside from the complex fabrication process for such structures. SIW and microstrip lines were used to design a 2 × 2 CP antenna [23,24]. However, both structures had low gain and efficiency. An 8 × 8 CP antenna array based on SIW is introduced with high gain and broad 3-dB AR [25]. However, the substrate losses had degraded its efficiency. In addition, manufacturing cost and simulating complexity increase by using a cavity layer to excite the radiating elements as subarrays of 2 × 2 elements. The cavity layer was mainly used because it was impossible to excite each element directly due to the SIW width [26–32]; therefore, the feed network cannot be designed in a single layer. As a result, these configurations have three layers: the backed cavity radiation layer and the feeding network layer. In addition, this kind of structure can dramatically increase the full-wave analysis processing time.

Here, an 8 × 8 high gain circular polarized array fed by a corporate feeding network based on PGWG is designed using the circularly polarized magneto-electric

dipole (CP-ME-dipole) as a radiating element [33]. Based on the concept of small to large finite arrays [34–36], the single feeding network is appropriately designed without needing a cavity layer with broad 3-dB AR, matching bandwidth, and excellent radiation performance.

The significant contribution of this article is related to the design of a CP antenna array, highlighting the necessity of designing the CP element in the array environment as the mutual coupling changes the amplitude ratio and the phase difference between the two components of the CP. A simple design of CP-ME-dipole is introduced based on a single port excitation with wideband performance. Such an element allows the design of a single layer of a cooperative feeding network based on load terminations, including the effect of mutual coupling and frequency variation rather than fixed identical frequency-independent loads. As all the loads are known, the feeding network is divided to reduce the number of optimization variables to speed up the optimization process. Thus, the design process is faster and reaches a practical design that agrees well with measured results. It should be pointed out that choosing a proper guiding structure for the 60 GHz band and millimeter wave frequencies in general is very important to having a highly efficient antenna system. Therefore, the printed-gap waveguide technology is adopted.

2. Design procedures

Designing a circularly polarized antenna array with good radiation performance and wideband requires first the design of the radiating element with a wide impedance and 3-dB AR bandwidths. Several radiating elements have been introduced to provide circular polarization. These designs provide a tradeoff between the impedance and AR bandwidths. For instance, a patch antenna with a cavity is used to generate a circularly polarized antenna; however, this element provides narrow impedance and AR bandwidths [22,23]. Also, a U-shaped slot antenna is used with wide bandwidth impedance and narrow AR bandwidths [20].

2.1. Isolated CP-ME-dipole

A wide-impedance ME-dipole was proposed, which exhibited excellent radiation characteristics regarding stable gain over the operating frequency [33]. The printed form of the ME-dipole consists of patches (electric dipole) on a substrate material; these patches are separated by slots (magnetic dipole). Circular polarization can be obtained by diagonally adding a metallic strip and trimming the corner of these patches, besides perturbing the geometry dimensions so the slot can excite two orthogonal linear modes with a phase shift of 90°.

A circular polarized ME-dipole (CO-ME-dipole) was used, where a wide impedance and 3-dB AR bandwidths were achieved [25], but the ME-dipole narrow slot was excited through an SIW cavity. A wideband CP antenna (impedance and AR bandwidths) eliminates the need for sequential feeding networks and avoids limiting the delay lines needed for sequential feeding. If such feeding is used in an array, it will require three layers of dielectric substrates and feeding subarrays of four elements. However, designing a parallel feeding network can be challenging. Therefore, in this article, the narrow slot of the CP-ME-dipole element is excited directly by a printed

gap waveguide (PGWG), as shown in **Figure 1**, avoiding using a cavity. Thus reducing the number of layers required to design and allowing each element's excitation in an array directly instead of the subarray used [25]. The pins layer is used to realize an AMC surface, force the electromagnetic waves to propagate following the printed line, and suppress around it over the pins. The line is printed on a dielectric substrate without the conventional ground plane, but the signal propagates above the microstrip and under the conducting plane that has the narrow slot. Rogers substrate, RO3003, with a relative dielectric constant of 3 and thickness of 0.13 mm, is used to be placed above the conducting pins, providing a band stop between 43 and 82 GHz. The printed CP-ME-dipole uses Rogers RO4003c substrate with a relative dielectric constant of 3.38 and a thickness of 0.508 mm.

The designed CP-ME-dipole has a wide impedance bandwidth of more than 15% for $|S_{11}| < -10$ dB (56–64 GHz) required for the 60-GHz frequency band, as shown in **Figure 2**. The 3-dB AR bandwidth is 25.9% (52.4–68 GHz), with a peak gain of 8.8 dBic, as elaborated in **Figure 2**. The radiation patterns for the two orthogonal planes indicate symmetric radiation patterns with almost constant beam width over their bandwidth. The co- and cross-polarization radiation patterns in the xz- and yz-plane at different frequencies (57, 60, and 64 GHz) are shown in **Figure 3**.

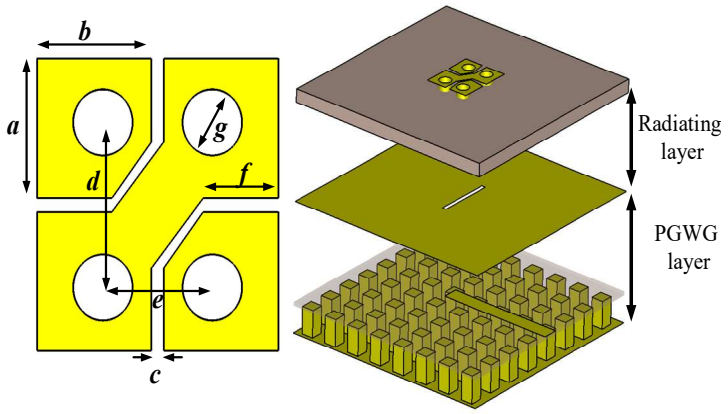

Figure 1. Schematic of the CP-ME-dipole with the PGWG (a = 0.976 mm, b = 0.896 mm, c = 0.096 mm, d = 1.137 mm, e = 0.85 mm, f = 0.565 mm and g = 0.44 mm).

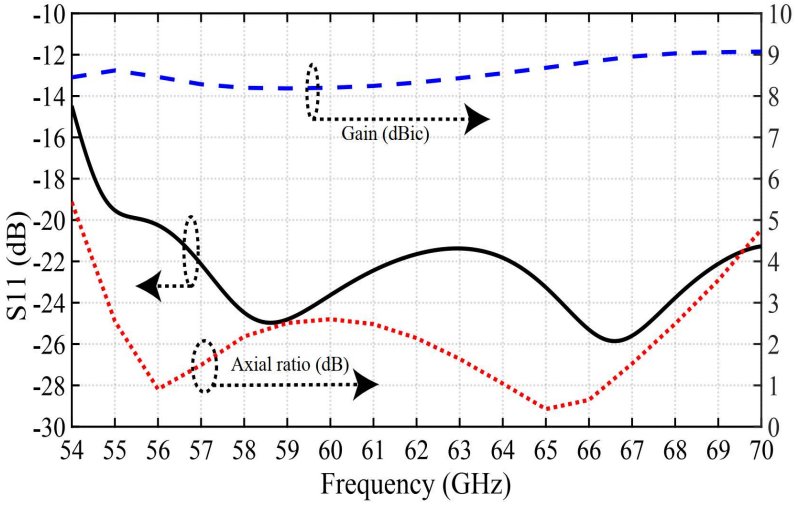

Figure 2. CP-ME-dipole antenna simulated S_{11}, gain, and AR.

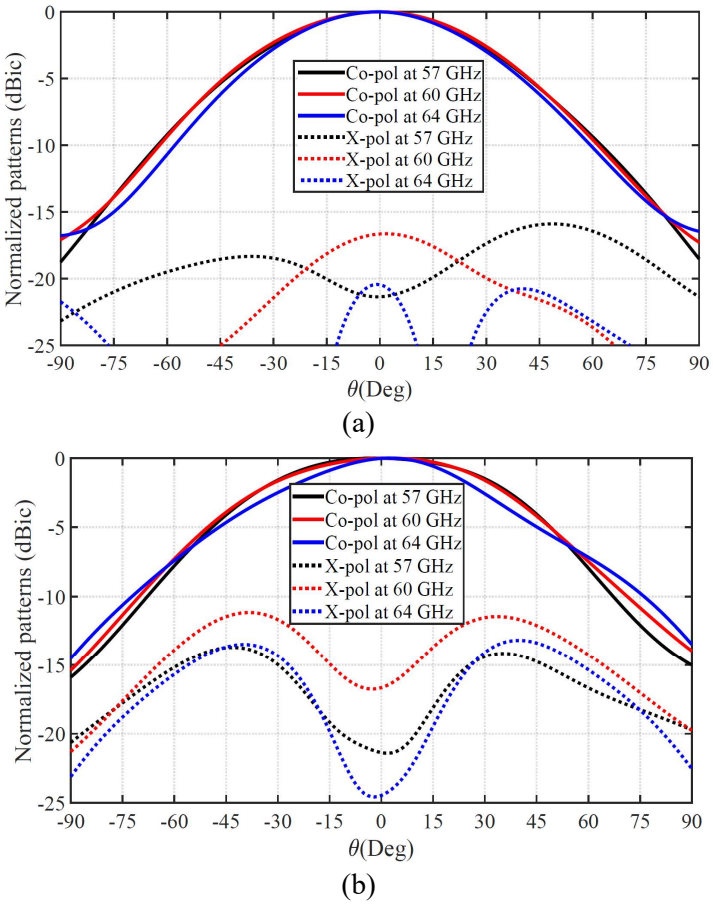

Figure 3. Simulated co- and cross-polar radiation patterns of a CP-ME-dipole antenna at different frequencies **(a)** xz-plane and **(b)** yz-plane.

2.2. Array design

Using the small-to-large array design procedure, a 4 ×4-element array in **Figure 1** is simulated without a feeding network. Unlike linearly polarized arrays, the CP arrays are critical to the amplitude and phase that affect the quality of the CP based on the AR level due to the coupling effect between the elements that are different in the x-direction than the y-direction (corresponding to E- and H-plane in the linearly polarized array).

Thus, the element parameters within the 4 × 4 array are tuned to fulfill the CP characteristics of AR less than 3 dB. The new parameters of the element in the 4 × 4 array environments in mm are $a = 1.02$, $b = 0.807$, $c = 0.117$, $d = 1.288$, $e = 0.699$, $f = 0.58$, and $g = 0.44$. With the new element, the 4 × 4 array is simulated without a feeding network to obtain the array S-matrix (Y-matrix or Z-matrix) at each frequency step. Then, the S-matrix of the proposed 8 × 8 array is predicted [35]. The 8 × 8 array arrangement and numbering are shown in **Figure 4**. From these S-parameters, the effective impedances of the 8 × 8 array are calculated for all frequencies required. A sample of these effective impedances is shown in **Figure 5** at 57, 60, and 64 GHz. It can be observed that the edge elements are extremely different from the middle elements, and the corner elements have the highest values.

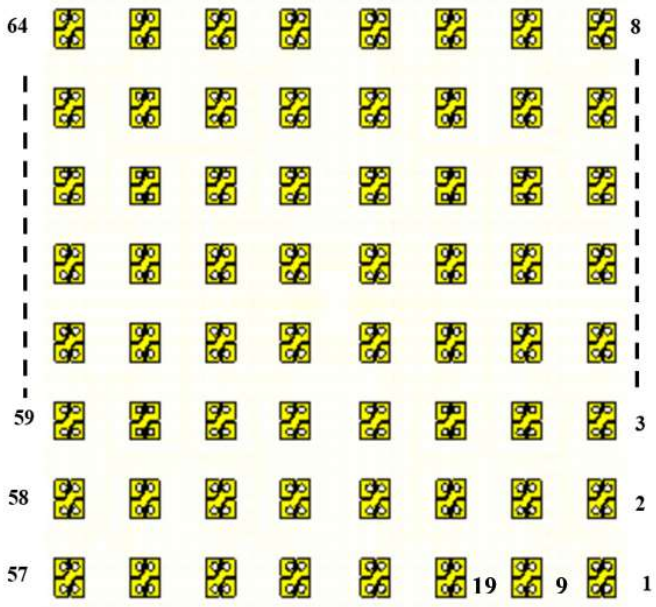

Figure 4. The 8 × 8 array elements are numbers from 1 to 64, as shown, starting from the lower right corner.

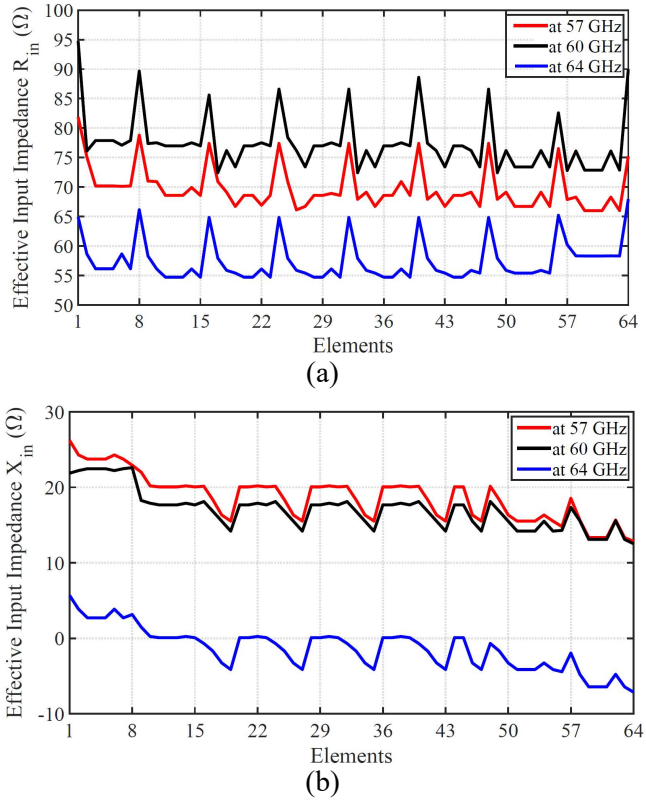

Figure 5. Predicted port effective impedance of an 8 × 8 array element from the 4 × 4 array elements at different frequencies **(a)** Real part and **(b)** Imaginary part.

The feeding network is designed based on the effective port impedances. However, when the feeding network is designed conventionally, as shown in **Figure 6** on the left side of a 2 × 2 elements, a direct coupling between the narrow slot and the close line (vertical midline) causes a change in the predicted input impedance and

the power distribution that did not account for such interaction. Of course, such interaction can be reduced by increasing the distance between the elements, which is not a desired solution because of the grating lobes. Thus, to center the line between the slots and keep the same distance between the radiating elements. The center line is tilted by an angle to achieve that, as shown on the right side in **Figure 6**. Such a change leads to a change in the layout of the cooperative feeding network, as shown in **Figure 7**. This network introduced two more power dividers (Power divider II and Power divider III) in addition to the conventional one (Power divider I). The power dividers used in **Figure 7** are shown in **Figure 8**. The S-parameters of the three power dividers after optimization are given in **Figure 9**.

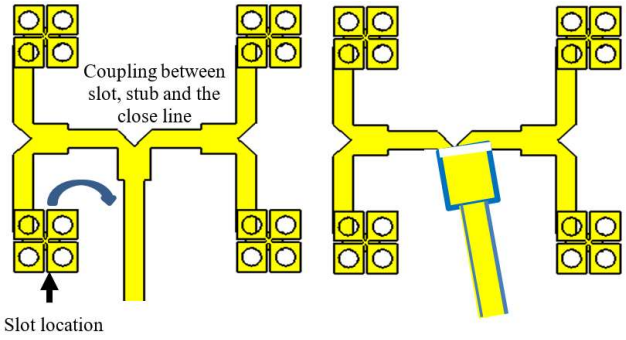

Figure 6. On the left side, a 2 × 2 array with a straight middle vertical line and the right side of the same array with a tilted middle line.

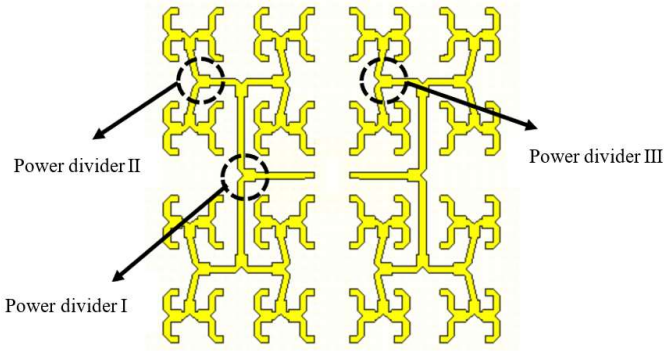

Figure 7. Layout of the modified feeding network for the 8 × 8 array.

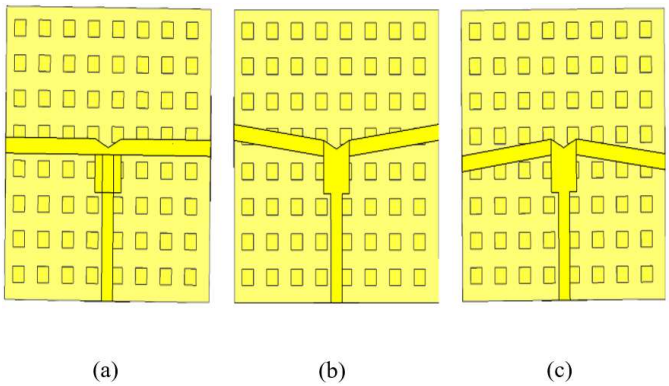

Figure 8. Sketch of different power dividers implemented in the printed feeding network: **(a)** Power divider I; **(b)** Power divider II; and **(c)** Power divider III.

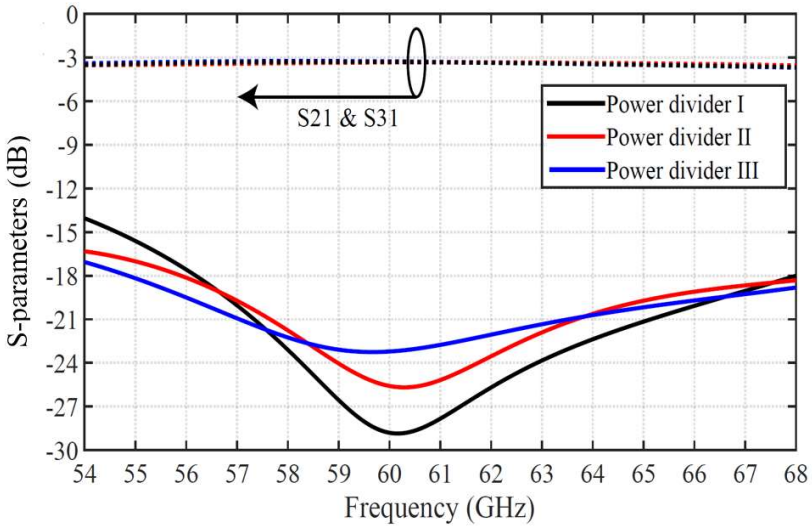

Figure 9. Simulated S-parameters of the power dividers in **Figure 8**.

After that, the feeding network is designed using the effective input impedances of the elements as terminated loads instead of the actual physical elements to reduce the full-wave analysis complexity for the feeding network optimization. The feeding network parameters are optimized, such as the line widths and the quarter-wavelength transformers for all lines. The feeding network and radiating layers are arranged, as shown in **Figure 10**. The feeding network layer consists of 3D printing EBG conducting pins similar to those presented [37] designed using PGWG, including the AMC pins. The electromagnetic signal is coupled between these two layers through slots etched on the top metal layer of the PGWG. PGWG allows the whole corporate feeding network to be designed in a single layer.

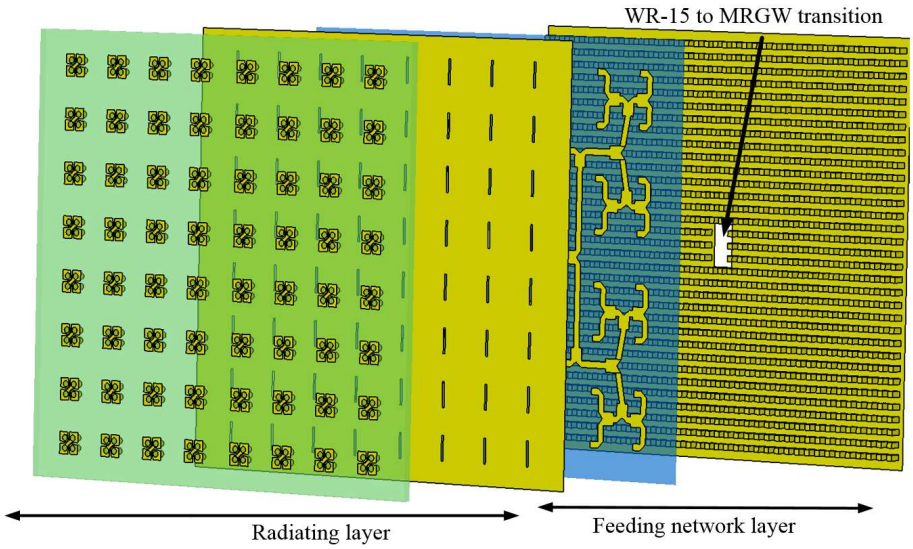

Figure 10. Different layers of the 8 × 8 array. The right layer is the EBG pins topped by a dielectric substrate with no conductor in the back, and the printed feeding network on top is separated from the top dielectric substrate by an air gap between the conducting surface with the slot arrays (forming the feeding network layer) feeding the ME-dipoles embedded in the dielectric substrate (forming the radiating elements layer).

3. Results

A physical prototype for the 8 × 8 array antenna is fabricated with a 37 × 37 mm^2 dimension. The bed of nails structure is connected from the back to a standard WR-15 flange [37]. It should be stated that the bed of nails is supposed to be about the same area as the array size. However, to reduce the cost of manufacturing, we have reused the bed nails used for the 16 x 16 elements [37]. Such a choice causes a reduction of the aperture efficiency due to using the ground plane size of the 16 × 16 array to predict the aperture efficiency. The 8 × 8 array of CP-ME-dipole elements fed by an optimized PGWG feeding network is fabricated, simulated, and measured. The photos of the top surface of these surfaces are shown in **Figure 11**. The $|S_{11}|$ is presented in **Figure 12**, showing a -10 dB reflection bandwidth of 18.3% (56.1 to 67 GHz) and 19.2% (56.4 to 68 GHz), respectively. The measured AR of the antenna array is also shown in **Figure 12**. Good agreement can be observed between the measurement and the simulation of S_{11} and AR.

The measured gain and radiation efficiency are shown in **Figure 13**, with a maximum gain of 26.2 dBic. Moreover, the radiation efficiency of the proposed antenna array is better than 82% over the operating frequency band. The measured gain shows about one dB less than the simulated gain, most likely due to higher dielectric losses and some fabrication tolerance. Furthermore, considering the 8 × 8 array dimensions of 37 × 37 mm^2 and the measured gain of 25.6 dBic, the aperture efficiency of the array is 52.8% at 60 GHz.

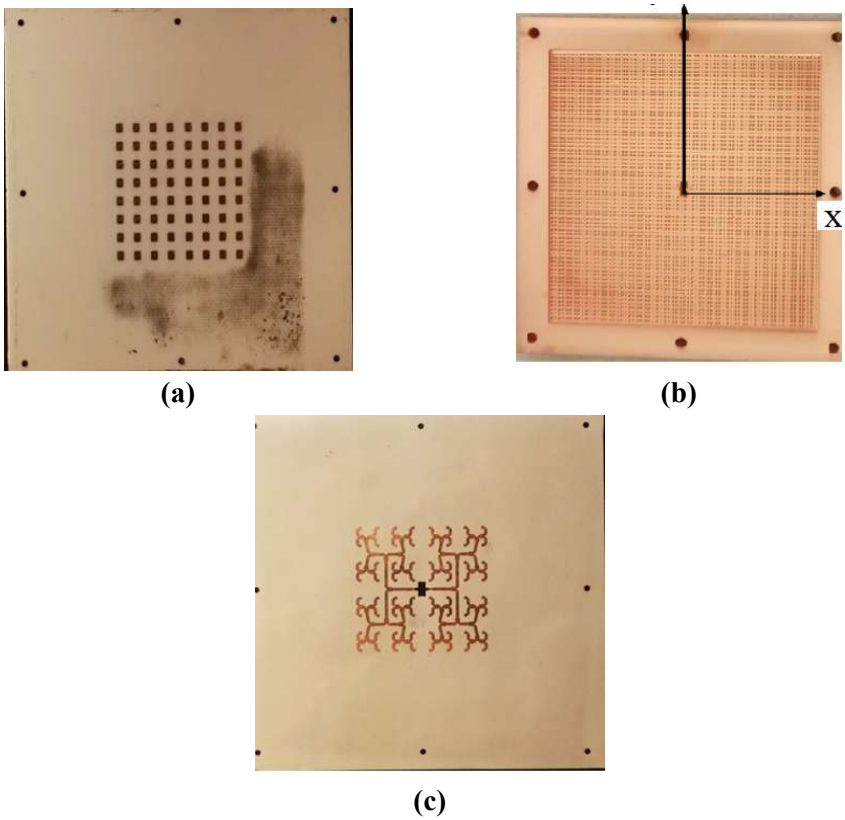

Figure 11. Photos of different layers of the antenna array. **(a)** Top view of the Pins used for a 16 × 16 array [37], **(b)** printed feeding network layer, and **(c)** radiating CP-ME-dipole array.

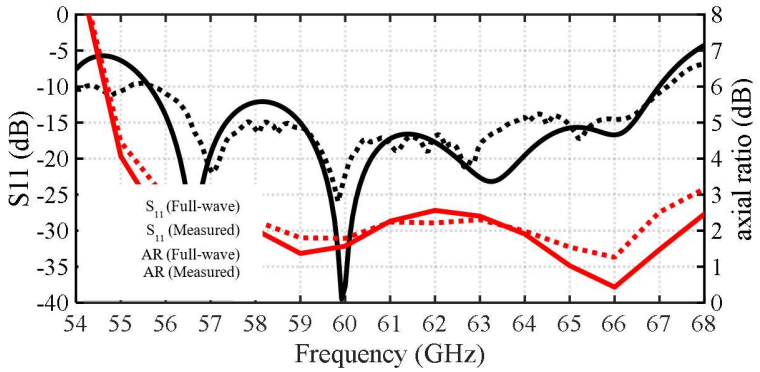

Figure 12. Simulated and measured S11 and AR of the antenna array.

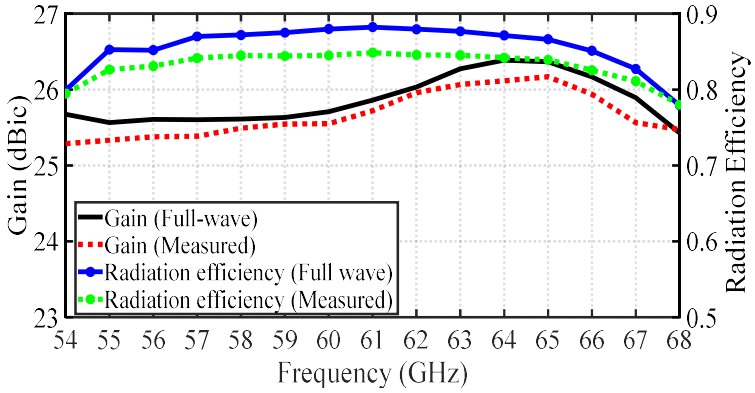

Figure 13. Simulated gain and radiation efficiency of the 8 × 8 antenna array.

Figures 14 and **15** show the antenna array's simulated and measured radiation patterns for 57, 60, and 64 GHz, respectively, in the xz- and yz-plane. The results show excellent agreement between the co-polar and x-polar radiation patterns at all frequencies within the whole elevation range. The power is distributed uniformly in phase and amplitude, so the first side lobe level should be around −13.6 GHz. However, the mutual coupling redistributes the power at some frequencies, giving the edge elements higher power than the central elements. Thus, the first sidelobe is higher than −13.6 dB, as shown at 57 GHz in **Figure 14a**. Also, a low cross-polarization level is achieved due to differential feeding between the array's two halves. The input port is the waveguide WR-15 from the back of the ground plane to the middle of the feeding network that divides the power equally but out of phase [37]. Thus, the two halves of the feeding network are 180 degrees from each other to compensate for the out-of-phase. Consequently, the cross-polarization is reduced.

A performance comparison of CP arrays operating in the 60-GHz band between arrays in the literature is reported in **Table 1**. Such comparison proves the different technologies used to design the elements and the feeding network. In addition, the performances of the arrays are given. The comparison indicates that the present design is compact and achieves better gain and radiation efficiency. Printed gap waveguide technology eliminates the need for a cavity layer [38]. Thus, the present array design with the PGWG feeding network makes the dielectric loss insignificant in the feeding network.

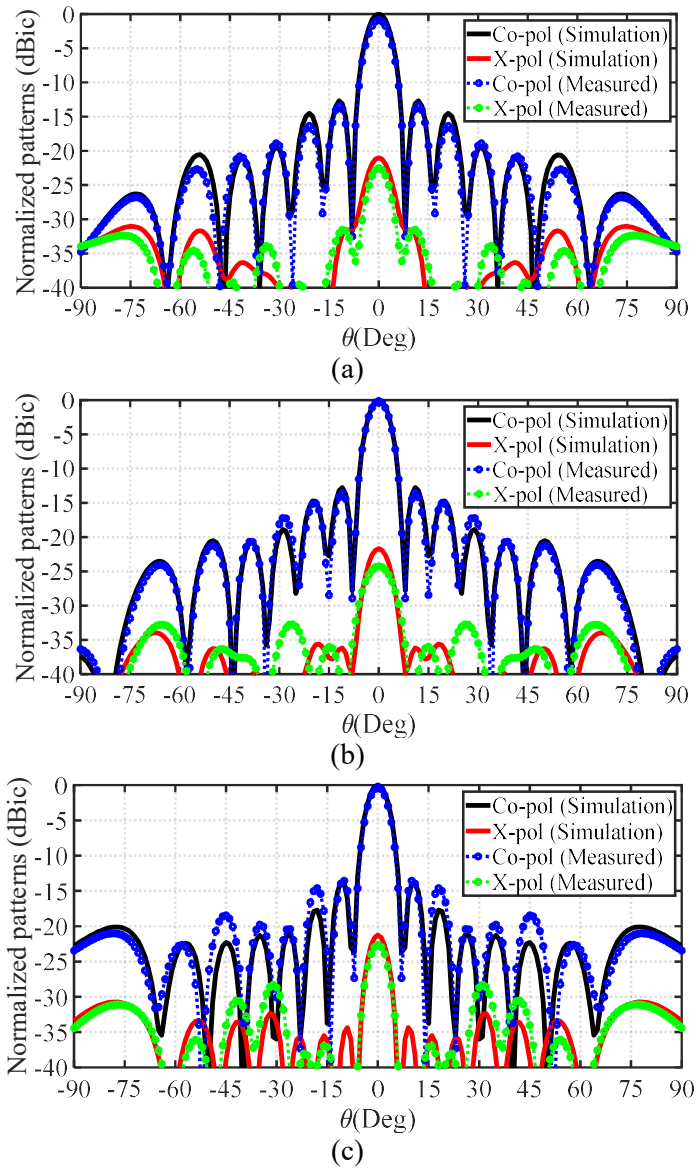

Figure 14. Radiation patterns in the xz-plane at **(a)** 57 GHz; **(b)** 60 GHz; and **(c)** 64 GHz.

Table 1. Performance comparison between the present array and some arrays operating in the 60 GHz band.

	Present	**[20]**	**[21]**	**[22]**	**[23]**	**[24]**	**[25]**
Size, mm^2	37^2	12.3^2	14 × 15.2	67.2^2	6.8 × 6.9	NA	30.6 × 34
NE	8 × 8	4 × 4	4×4	16 × 16	2 × 2	2 × 2	8 × 8
NL	2	2	2	3	3	2	3
FNT	PGWG	ST	CPW	WG	SIW	ST	SIW
BW %	18.3	28.1	17.8	5.7	6.7	15.9	18.2
G, dBic	26.2	16	16	33.3	12.2	11.43	26.1
η	>82	>52.5	>34.9	>89.6	>70	NA	>70
AR %	19.8	19.2	15.6	6.4	6.8	15.9	16.5

Abbreviations in the Table: stripline (ST), Substrate waveguide (SIW), Coplanar waveguide (CPW), Waveguide (WG), number of elements (NE), number of layers (NL), Radiation efficiency (η), Feeding Network Technology (FNT), gain (G), Bandwidth (BW).

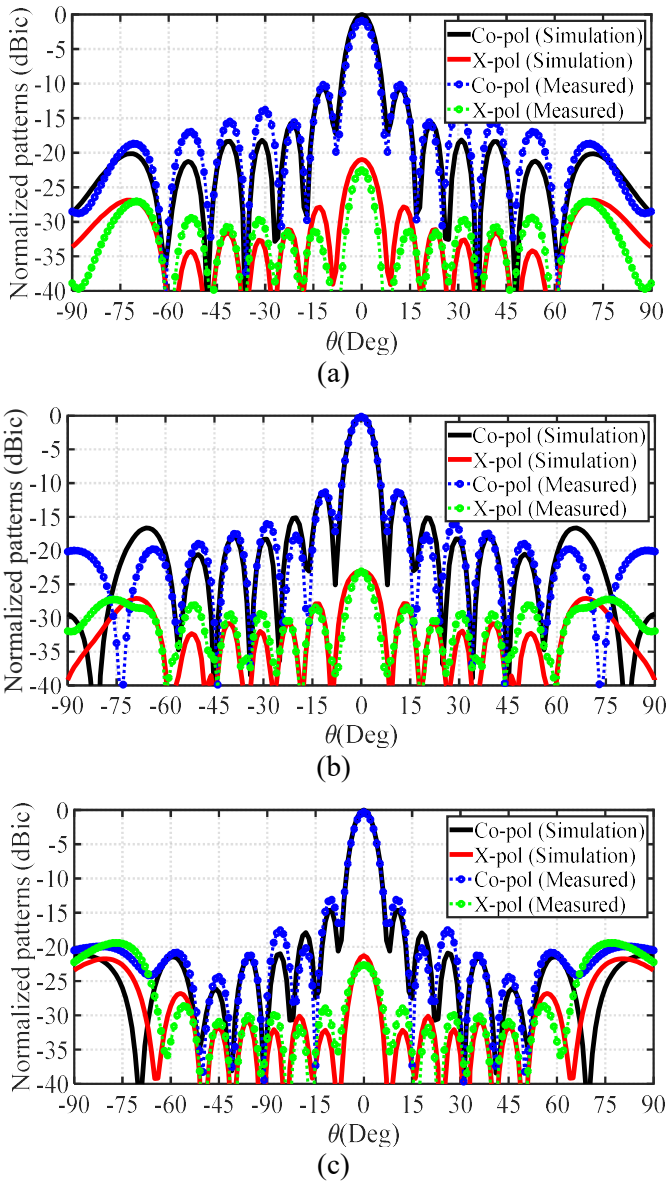

Figure 15. Radiation patterns in the yz-plane at **(a)** 57 GHz; **(b)** 60 GHz; and **(c)** 64GHz.

4. Conclusion

A new concept for designing a circularly polarized antenna array, including the mutual coupling effect, has been introduced. A compact 8 × 8 antenna array with a single layer of feeding network has been proposed for high-gain circular polarization. A wide AR bandwidth has been achieved using the CP-ME-dipole radiating element without sequential feeding. Furthermore, the proposed array designs have high radiation efficiency due to the use of the PGWG for designing a full-corporate feeding network, which could be an excellent candidate for future millimeter-wave wireless and 5G applications.

Author contributions: Conceptualization, ATH, and AAK; methodology, AAK; software, ATH and AAK; validation, ATH; formal analysis, ATH; investigation, ATH; resources, AAK; data curation, ATH; writing—original draft preparation, ATH; writing—review and editing,

AAK; visualization, ATH; supervision, AAK; project administration, AAK; funding acquisition, AAK. All authors have read and agreed to the published version of the manuscript.

Funding: The CRCP supported this work under the award number CRC-201700172.

Conflict of interest: The authors declare no conflict of interest.

References

1. Smulders P. Exploiting the 60 GHz band for local wireless multimedia access: prospects and future directions. IEEE Communications Magazine. 2002; 40(1): 140-147. doi: 10.1109/35.978061
2. Rappaport TS, Xing Y, MacCartney GR, et al. Overview of Millimeter Wave Communications for Fifth-Generation (5G) Wireless Networks—With a Focus on Propagation Models. IEEE Transactions on Antennas and Propagation. 2017; 65(12): 6213-6230. doi: 10.1109/tap.2017.2734243
3. Lockie D, Peck D. High-data-rate millimeter-wave radios. IEEE Microwave Magazine. 2009; 10(5): 75-83. doi: 10.1109/mmm.2009.932834
4. Zheng K, Zhao L, Mei J, et al. 10 Gb/s hetsnets with millimeter-wave communications: access and networking - challenges and protocols. IEEE Communications Magazine. 2015; 53(1): 222-231. doi: 10.1109/mcom.2015.7010538
5. Rangan S, Rappaport TS, Erkip E. Millimeter-Wave Cellular Wireless Networks: Potentials and Challenges. Proceedings of the IEEE. 2014; 102(3): 366-385. doi: 10.1109/jproc.2014.2299397
6. Manabe T, Sato K, Masuzawa H, et al. Polarization dependence of multipath propagation and high-speed transmission characteristics of indoor millimeter-wave channel at 60 GHz. IEEE Transactions on Vehicular Technology. 1995; 44(2): 268-274. doi: 10.1109/25.385918
7. Hirokawa J, Ando M. Efficiency of 76-GHz post-wall waveguide-fed parallel-plate slot arrays. IEEE Transactions on Antennas and Propagation. 2000; 48(11): 1742-1745. doi: 10.1109/8.900232
8. Hirokawa J, Ando M. Single-layer feed waveguide consisting of posts for plane TEM wave excitation in parallel plates. IEEE Transactions on Antennas and Propagation. 1998; 46(5): 625-630. doi: 10.1109/8.668903
9. Deslandes D, Wu K. Integrated microstrip and rectangular waveguide in planar form. IEEE Microwave and Wireless Components Letters. 2001; 11(2): 68-70. doi: 10.1109/7260.914305
10. Li Y, Luk KM. Low-Cost High-Gain and Broadband Substrate- Integrated-Waveguide-Fed Patch Antenna Array for 60-GHz Band. IEEE Transactions on Antennas and Propagation. 2014; 62(11): 5531-5538. doi: 10.1109/tap.2014.2350509
11. Li Y, Luk KM. 60-GHz Substrate Integrated Waveguide Fed Cavity-Backed Aperture-Coupled Microstrip Patch Antenna Arrays. IEEE Transactions on Antennas and Propagation. 2015; 63(3): 1075-1085. doi: 10.1109/tap.2015.2390228
12. Zhao Y, Luk KM. Dual Circular-Polarized SIW-Fed High-Gain Scalable Antenna Array for 60 GHz Applications. IEEE Transactions on Antennas and Propagation. 2018; 66(3): 1288-1298. doi: 10.1109/tap.2018.2797530
13. Wang L, Yin X, Li S, et al. Phase Corrected Substrate Integrated Waveguide H-Plane Horn Antenna With Embedded Metal-Via Arrays. IEEE Transactions on Antennas and Propagation. 2014; 62(4): 1854-1861. doi: 10.1109/tap.2014.2298042
14. Wang L, Yin X, Esquius-Morote M, et al. Circularly Polarized Compact LTSA Array in SIW Technology. IEEE Transactions on Antennas and Propagation. 2017; 65(6): 3247-3252. doi: 10.1109/tap.2017.2696955
15. Li T, Chen ZN. Control of Beam Direction for Substrate-Integrated Waveguide Slot Array Antenna Using Metasurface. IEEE Transactions on Antennas and Propagation. 2018; 66(6): 2862-2869. doi: 10.1109/tap.2018.2823755
16. Li T, Chen ZN. A Dual-Band Metasurface Antenna Using Characteristic Mode Analysis. IEEE Transactions on Antennas and Propagation. 2018; 66(10): 5620-5624. doi: 10.1109/tap.2018.2860121
17. Kildal PS. Three metamaterial-based gap waveguides between parallel metal plates for mm/submm waves. In: Proceedings of the 2009 3rd European Conference on Antennas and Propagation; 23–27 March 2009; Berlin, Germany. pp. 28-32.
18. Zaman AU, Kildal PS. Gap waveguides. In: Chen ZN, Liu D, Nakano H, et al. (editors). Handbook of Antenna Technologies. Springer; 2016. pp. 3273-3347.
19. Zaman AU, Kildal PS. Different gap waveguide slot array configurations for mmwave fixed beam antenna application. In: Proceedings of the 2016 10th European Conference on Antennas and Propagation (EuCAP); 10–15 April 2016; Davos, Switzerland. pp. 1-4. doi: 10.1109/eucap.2016.7481541

20. Sun H, Guo YX, Wang Z. 60-GHz Circularly Polarized U-Slot Patch Antenna Array on LTCC. IEEE Transactions on Antennas and Propagation. 2013; 61(1): 430-435. doi: 10.1109/tap.2012.2214018
21. Li M, Luk KM. Low-Cost Wideband Microstrip Antenna Array for 60-GHz Applications. IEEE Transactions on Antennas and Propagation. 2014; 62(6): 3012-3018. doi: 10.1109/tap.2014.2311994
22. Miura Y, Hirokawa J, Ando M, et al. A circularly-polarized aperture array antenna with a corporate-feed hollow-waveguide circuit in the 60 GHz-band. In: Proceedings of the 2011 IEEE International Symposium on Antennas and Propagation (APSURSI); 3–8 July 2011; Spokane, WA, USA. pp. 3029-3032. doi: 10.1109/aps.2011.5997168
23. Guntupalli AB, Ke Wu. 60-GHz Circularly Polarized Antenna Array Made in Low-Cost Fabrication Process. IEEE Antennas and Wireless Propagation Letters. 2014; 13: 864-867. doi: 10.1109/lawp.2014.2320906
24. Sun YX, Leung KW. Circularly Polarized Substrate-Integrated Cylindrical Dielectric Resonator Antenna Array for 60 GHz Applications. IEEE Antennas and Wireless Propagation Letters. 2018; 17(8): 1401-1405. doi: 10.1109/lawp.2018.2847295
25. Li Y, Luk KM. A 60-GHz Wideband Circularly Polarized Aperture-Coupled Magneto-Electric Dipole Antenna Array. IEEE Transactions on Antennas and Propagation. 2016; 64(4): 1325-1333. doi: 10.1109/tap.2016.2537390
26. Miura Y, Hirokawa J, Ando M, et al. Double-Layer Full-Corporate-Feed Hollow-Waveguide Slot Array Antenna in the 60-GHz Band. IEEE Transactions on Antennas and Propagation. 2011; 59(8): 2844-2851. doi: 10.1109/tap.2011.2158784
27. Li Y, Luk KM. Low-Cost High-Gain and Broadband Substrate- Integrated-Waveguide-Fed Patch Antenna Array for 60-GHz Band. IEEE Transactions on Antennas and Propagation. 2014; 62(11): 5531-5538. doi: 10.1109/tap.2014.2350509
28. Li Y, Luk KM. 60-GHz Substrate Integrated Waveguide Fed Cavity-Backed Aperture-Coupled Microstrip Patch Antenna Arrays. IEEE Transactions on Antennas and Propagation. 2015; 63(3): 1075-1085. doi: 10.1109/tap.2015.2390228
29. Liu J, Vosoogh A, Zaman AU, Kildal PS. Design of a cavity backed slot array unit cell on inverted microstrip gap waveguide. In: Proceedings of the 2015 International Symposium on Antennas and Propagation (ISAP); 9–12 November 2015; Hobart, TAS, Australia. pp. 1-4.
30. Liu J, Vosoogh A, Zaman AU, Kildal PS. Design of 8 × 8 slot array antenna based on inverted microstrip gap waveguide. In: Proceedings of the 2016 International Symposium on Antennas and Propagation (ISAP); 24–28 October 2016; Okinawa, Japan. pp. 760-761.
31. Liu J, Vosoogh A, Zaman AU, et al. Design and Fabrication of a High-Gain 60-GHz Cavity-Backed Slot Antenna Array Fed by Inverted Microstrip Gap Waveguide. IEEE Transactions on Antennas and Propagation. 2017; 65(4): 2117-2122. doi: 10.1109/tap.2017.2670509
32. Farahbakhsh A, Zarifi D, Zaman AU. 60-GHz Groove Gap Waveguide Based Wideband H -Plane Power Dividers and Transitions: For Use in High-Gain Slot Array Antenna. IEEE Transactions on Microwave Theory and Techniques. 2017; 65(11): 4111-4121. doi: 10.1109/tmtt.2017.2699680
33. Luk KM, Wong H. A new wideband unidirectional antenna element. International Journal of Microwave and Optical Technology. 2006; 1(1): 35-44.
34. Ahmed AK. Design of Large Finite Arrays Using Simulations or Measurements of Small Arrays. Forum for Electromagnetic Research Methods and Application Technologies (FERMAT). 2014.
35. Kishk AA. Prediction of large array characteristics from small array parameters. In: Proceedings of the 2nd European Conference on Antennas and Propagation (EuCAP 2007); 11-16 November 2007; Edinburgh, UK. doi: 10.1049/ic.2007.1111
36. Kishk AA, Hassan AT. Design of Large Finite Array Antennas and its Feeding Network. In: Proceedings of the 2019 IEEE International Conference on Computational Electromagnetics (ICCEM); 20-22 March 2019; Shanghai, China. pp. 1-3. doi: 10.1109/compem.2019.8779178
37. Hassan AT, Kishk AA. Efficient Procedure to Design Large Finite Array and Its Feeding Network With Examples of ME-Dipole Array and Microstrip Ridge Gap Waveguide Feed. IEEE Transactions on Antennas and Propagation. 2020; 68(6): 4560-4570. doi: 10.1109/tap.2020.2972407
38. Vosoogh A, Sorkherizi MS, Zaman AU, et al. An Integrated Ka-Band Diplexer-Antenna Array Module Based on Gap Waveguide Technology With Simple Mechanical Assembly and No Electrical Contact Requirements. IEEE Transactions on Microwave Theory and Techniques. 2018; 66(2): 962-972. doi: 10.1109/tmtt.2017.2757469